Measuring neutron spectra in radiotherapy using the nested neutron spectrometer

Robert Maglieri[a)]
Medical Physics Unit, McGill University, Montreal, Quebec H4A 3J1, Canada

Angel Licea
Canadian Nuclear Safety Commission, Ottawa, Ontario K1P 5S9, Canada

Michael Evans, Jan Seuntjens, and John Kildea
Medical Physics Unit, McGill University, Montreal, Quebec H4A 3J1, Canada

(Received 29 March 2015; revised 28 August 2015; accepted for publication 13 September 2015; published 7 October 2015)

Purpose: Out-of-field neutron doses resulting from photonuclear interactions in the head of a linear accelerator pose an iatrogenic risk to patients and an occupational risk to personnel during radiotherapy. To quantify neutron production, in-room measurements have traditionally been carried out using Bonner sphere systems (BSS) with activation foils and TLDs. In this work, a recently developed active detector, the nested neutron spectrometer (NNS), was tested in radiotherapy bunkers.
Methods: The NNS is designed for easy handling and is more practical than the traditional BSS. Operated in current-mode, the problem of pulse pileup due to high dose-rates is overcome by measuring current, similar to an ionization chamber. In a bunker housing a Varian Clinac 21EX, the performance of the NNS was evaluated in terms of reproducibility, linearity, and dose-rate effects. Using a custom maximum-likelihood expectation–maximization algorithm, measured neutron spectra at various locations inside the bunker were then compared to Monte Carlo simulations of an identical setup. In terms of dose, neutron ambient dose equivalents were calculated from the measured spectra and compared to bubble detector neutron dose equivalent measurements.
Results: The NNS-measured spectra for neutrons at various locations in a treatment room were found to be consistent with expectations for both relative shape and absolute magnitude. Neutron fluence-rate decreased with distance from the source and the shape of the spectrum changed from a dominant fast neutron peak near the Linac head to a dominant thermal neutron peak in the moderating conditions of the maze. Monte Carlo data and NNS-measured spectra agreed within 30% at all locations except in the maze where the deviation was a maximum of 40%. Neutron ambient dose equivalents calculated from the authors' measured spectra were consistent (one standard deviation) with bubble detector measurements in the treatment room.
Conclusions: The NNS may be used to reliably measure the neutron spectrum of a radiotherapy beam in less than 1 h, including setup and data unfolding. This work thus represents a new, fast, and practical method for neutron spectral measurements in radiotherapy. [http://dx.doi.org/10.1118/1.4931963]

Key words: neutrons, neutron spectroscopy, Monte Carlo, MLEM, NNS

1. INTRODUCTION

During high-energy radiotherapy treatments (>10 MV), neutrons are produced in the head of the Linac through photonuclear interactions.[1] These photoneutrons contribute to the accepted, yet unwanted, out-of-field doses that pose an iatrogenic risk to patients and an occupational risk to personnel.[2] Such risks are attributed to the large quality factor of neutrons (compared to photons) and may give rise to many health concerns, particularly the induction of secondary cancers.[3]

To understand and mitigate the risk from photoneutrons during radiotherapy treatments, the neutron energy spectrum should be quantified. There are many methods to measure neutron spectra including nuclear recoil, velocity measurements, threshold methods, and multisphere measurements.[4] In radiotherapy, a common technique is to make use of the Bonner sphere system (BSS).[5] The BSS consists of a central thermal neutron detector surrounded by different sized spheres of hydrogenous material (moderators).

Traditionally, passive neutron detectors such as gold activation foils[6] and thermoluminescent detectors[7] have been used with the BSS. While these detectors generally produce good results, passive detectors require an additional step to "readout" data after the experiment, adding to the overall measurement time. Active detectors, on the other hand, are not generally used with the BSS because of the pulsed nature and high dose-rates of radiotherapy beams. This leads to a pulse pileup problem within the multichannel analyzer (MCA) and is a major obstacle to overcome.

In this work, we have validated the use of a new neutron spectrometer, known as the nested neutron spectrometer (NNS) produced by Dubeau,[8] for active measurements within

a radiotherapy bunker. The NNS is a neutron spectrometer that is operated on the same principle as the well-established BSS but is more practical for field measurements. The problem of pulse pileup was solved by operating the spectrometer in current readout mode similar to that used with an ionization chamber–electrometer combination.

2. MATERIALS AND METHODS

2.A. Nested neutron spectrometer

A schematic view of the NNS is shown in Fig. 1. It consists of a central He-3 detector and seven cylindrical high-density polyethylene (HDPE) moderators (0.945 g/cm^3) assembled in Russian doll fashion. Since He-3 is mainly sensitive to thermal neutrons, the addition of each successive moderator yields a different response to the neutron spectrum being measured. Combining the different responses, an unfolding algorithm then reconstructs the neutron spectrum.

The He-3 detector is filled with 2 atm of He-3 and 0.7 atm of krypton added as a quenching gas. In the event that a photon background signal is large compared to the neutron signal, a He-4 detector, with the same photon response as the He-3 detector but insensitive to neutrons, may be used to measure the photon background. The photon signal can thus be subtracted leaving a neutron-only signal.

The moderators have diameters ranging from 6 to 22 cm and were designed to match the response of a BSS. A small hole in the center of each cap facilitates readout of the detector signal. Measurements are carried out with the NNS placed either on a variable height tripod or on an adjustable aluminum shelf ensuring that the position of the detector's sensitive volume remains the same position during measurements.

2.A.1. Operation

The NNS may be operated in pulse-mode, Fig. 2(a), as a proportional counter with a MCA or in current-mode,

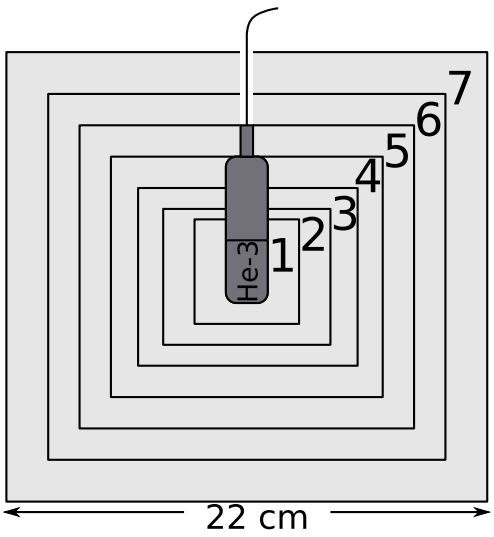

FIG. 1. Schematic cross section of the cylindrical NNS system showing the detector and all seven moderators. The He-3 detector's sensitive volume is positioned at the center of the moderator combination.

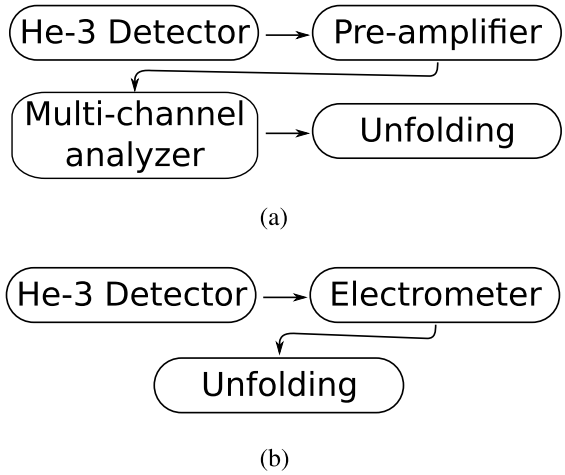

FIG. 2. Operational modes of the nested neutron spectrometer: (a) pulse-mode as a proportional counter counting pulse and (b) current-mode as an ionization chamber measuring current.

Fig. 2(b), as an ionization chamber with an electrometer. In pulse-mode, the pulse-height spectrum for each moderator is integrated to obtain the total neutron counts. For count-rates above the limit of the MCA (~10 000 counts/s), this method breaks down due to pulse pileup and increased dead time. Conversely, current-mode solves the problem of pulse pileup since individual pulses are no longer counted. In this mode, the measured current is converted to corresponding count-rate through a calibration coefficient (see Table I). This is possible because the neutron current is proportional to the neutron fluence-rate for a given situation. In addition, any contributions from photons are subtracted off using the He-4. This mode of operation is based on the principle outlined by Hagiwara *et al.*[9]

Before every measurement, a leakage test is performed to evaluate the magnitude of the leakage current which is then subtracted from the total charge after measurement. In both modes of operation, the count-rate combined with the response functions for each moderator allows us to calculate the neutron spectrum through mathematical unfolding.

2.A.2. Response functions

Response functions, as generated by the vendor using the Monte Carlo N-Particle code,[10] for the bare detector and

TABLE I. Verification of calibration coefficient 7.0 fA/(counts/s) using a 5 Ci Am-Be source at the neutron laboratory of the Canadian Nuclear Safety Commission.

Moderator	Pulse-mode (counts/s)	Current-mode (fA)	Coefficient [fA/(counts/s)]
7	83.83	692	8.3
6	99.15	720	7.3
5	89.53	619	6.9
4	76.87	598	7.8
3	59.23	566	9.6
2	49.82	444	8.9
1	38.21	233	6.1
Average	—	—	7.8 ± 1.2

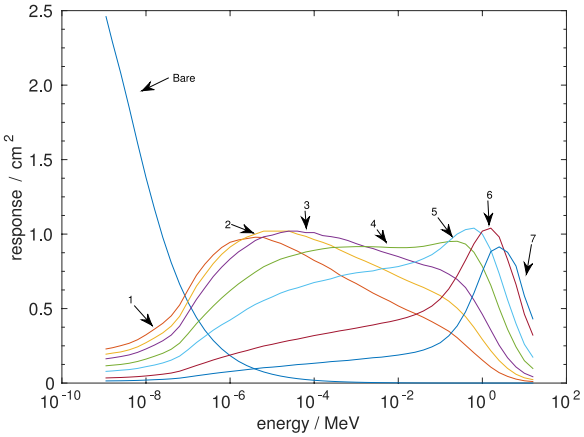

FIG. 3. Response curves for the NNS. Each moderator is indicated by integers 1–7; the smallest integer represents the smallest moderator.

the seven moderators are shown in Fig. 3. They represent the amount of (*n*,*p*) reactions in He-3. These response functions were not reproduced in this work as the exact dimensions and composition of the moderators were unavailable.

2.A.3. Calibration

Because the response functions incorporate the count-rate, current-mode measurements must first be converted to count-rate before unfolding. The vendor-supplied current to count-rate conversion coefficient for our NNS unit was 7 fA/(counts/s). We experimentally confirmed this number at the neutron laboratory of the Canadian Nuclear Safety Commission in Ottawa. Table I presents the current and count-rates we measured using the CNSC's Am-Be source. The experimental setup was identical between the current-mode and pulse-mode measurements. No additional He-4 correction measurements were needed due to the negligible photon background.

2.B. Maximum-likelihood expectation–maximization (MLEM) unfolding

To unfold the raw data, we developed a user-friendly MLEM algorithm by which we deconvolved the eight measurements, one per moderator and the bare detector, into a 52-bin neutron energy spectrum. The deconvolution problem can be described as follows: if m_i is the measurement of the i-th moderator, $A_i(E)$ is the response function of the i-th moderator as a function of energy, and $n(E)$ is the neutron spectrum to be found, then m_i is related to $n(E)$ by a Fredholm integral of the first kind,

$$m_i(E) = \int_E^{E+\Delta E} A_i(E')n(E')dE'. \quad (1)$$

Equation (1) can be directly integrated by discretization using the MLEM technique. MLEM is a standard statistical reconstruction tool that is commonly used in positron emission tomography (PET).[11] When applied to convergence, the MLEM algorithm maximizes the likelihood of obtaining the measured data m given that the spectrum is n and is described as follows:

$$n_j^{k+1} = \frac{n_j^k}{\sum_{i=1}^{N} a_{ij}} \sum_{i=1}^{N} a_{ij} \frac{m_i}{\sum_{b=1}^{J} a_{ib} n_b^k}. \quad (2)$$

Here, n_b^k is the starting spectrum, n_j^k is the current spectrum estimate, a_{ij} is the response function of the detector, and m_i is the measurement in counts per second.

The MLEM algorithm always converges. However, if no stopping criterion is applied, it will run indefinitely and acquire noise. Therefore, a stopping criterion is introduced to halt the algorithm when the difference between the measured data and the reconvolved spectrum, $m_i - \sum_j^n a_{ij} n_j$, reaches a minimum value. In the event that noise overtakes the algorithm as a result of poor data, a hard cutoff is set at 10 000 iterations of the algorithm.

As described below, our MLEM algorithm was validated for neutron spectrum unfolding using reference sources and by comparison with the vendor-supplied STAY'SL algorithm.[12]

2.C. Measurement uncertainties

Statistical uncertainties on the measurements were estimated using a random sampling process. For each of the eight count-rate measurements, we assumed the measured values represented the mean and standard deviation of a Poisson distribution. Sampling a random value from these distributions, a new pseudo-measurement set was created and unfolded. Iterating this method 50 times and averaging the spectra, we obtained a sampled neutron spectrum that includes statistical fluctuations as well as variations in the unfolding process. The final estimate of uncertainty is represented by the root mean square difference between the sampled neutron spectrum and the measured neutron spectrum.

2.D. MLEM validation

The NNS was validated by the vendor in various reference neutron fields including D_2O-moderated and unmoderated Cf-252 sources at the National Institute of Standards and Technology (NIST) and an Am-Be source at the National Research Council Canada (NRC).[8] We validated our MLEM algorithm by applying it to vendor-acquired raw data and comparing the results to vendor-unfolded spectra. Figure 4 presents the vendor's moderated Cf-252 spectrum, unfolded using the STAY'SL algorithm, together with our MLEM-unfolded spectrum for the same dataset. There is a small thermal peak due to scatter in the room.[13,14] The two spectra agree very well including scatter components. In addition, the total fluence-rate was calculated for each case and determined to be 399.9 and 400.1 n cm^{-2} s^{-1} for the STAY'SL and MLEM algorithms. As shown in Fig. 5, our unfolded Cf-252 spectrum also compares well to the ISO 8529-2 Cf-252 reference spectrum,[15] providing further validation of the MLEM algorithm for neutron spectrum unfolding. The starting spectra used for the comparison of each algorithm

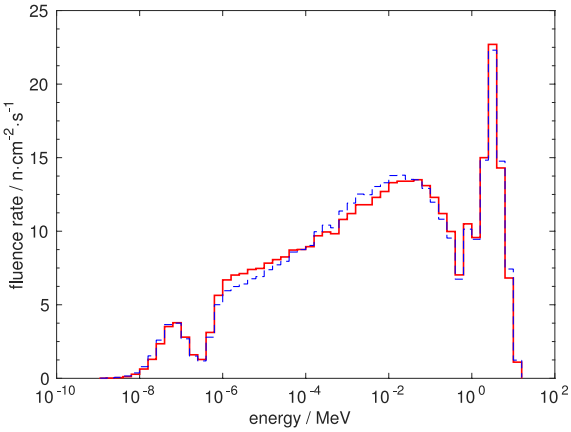

FIG. 4. Comparison of the MLEM- (solid line) and STAY'SL-reconstructed (dashed line) neutron spectrum of a D_2O-moderated Cf-252 neutron source.

were identical and comprised Monte Carlo data provided to the vendor by NIST.

2.E. Performance testing in a radiotherapy environment

Making use of a Varian Clinac 21EX Linac (Varian Medical Systems, Palo Alto, CA) at the Montreal General Hospital (McGill University Health Center, Montreal, PQ), we evaluated the NNS on three performance tests: reproducibility, linearity, and dose-rate. For each test, the jaws of the Linac were closed, the gantry was aimed at the floor, and the NNS was placed on the couch at 40 cm from the isocenter with the center of the sensitive volume at the height of the isocenter. In this setup, the photon component, as measured using the He-4 detector, was low as compared to the neutron signal and ignored. Figure 6 provides a photo of the setup.

To test reproducibility, three measurements of 600 monitor units (MU) at 600 MU/min yielded standard deviations in each moderator less than 1% of the mean value. Next, linearity was tested by varying total dose from 600 to 1800 MU; count-rates were within 1% of the baseline values for each moderator at 600 MU. Finally, dose-rate effects were studied by changing

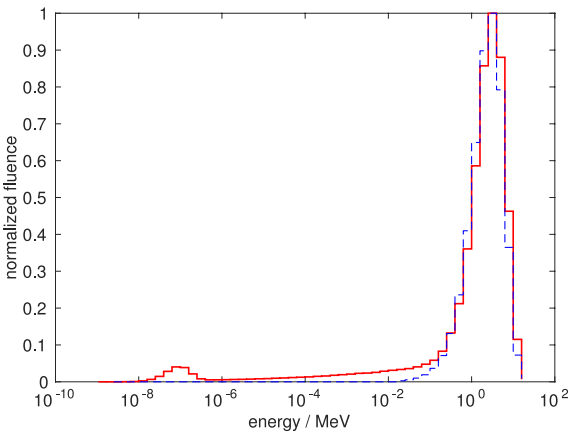

FIG. 5. Comparison of the MLEM-reconstructed (solid line) measured data and ISO-8529-2 reference spectrum (dashed line) of a Cf-252 neutron source. A thermal neutron peak is present for the NNS-measured data due to room scatter.

FIG. 6. Nested neutron spectrometer with sensitive volume at 40 cm from the Linac isocenter of a Varian 21EX Linac at the Montreal General Hospital. All seven moderators are present.

the photon dose-rate from 600 to 400 MU/min; total neutron fluence-rates varied from 1.21×10^6, and 0.81×10^6 n cm^{-2} s^{-1} for 600 and 400 MU/min, respectively. The ratio of the two fluence-rates equals that of the dose-rates.

Given the cylindrical shape of the moderators, a directional dependence may be expected. In the work of Dubeau *et al.*,[8] the authors observed an 8% change in response from a simulated point source in line with the He-3 detector axis when the NNS was rotated by 90°. However, in radiotherapy, the radiation field in the bunker is similar to that of a neutron bath with radiation arriving isotropically at the detector.[3] We can thus assume that the directional dependence is negligible outside of a direct radiotherapy beam.

2.E.1. Measuring radiotherapy photoneutron spectra

Figure 7 shows the location of NNS measurements in the bunker of our Varian Clinac 21EX Linac. Measurement locations were chosen to be consistent with the work of the previous authors[6,16] and to show the effect of neutron moderation in the maze. The Linac was operated at 18 MV

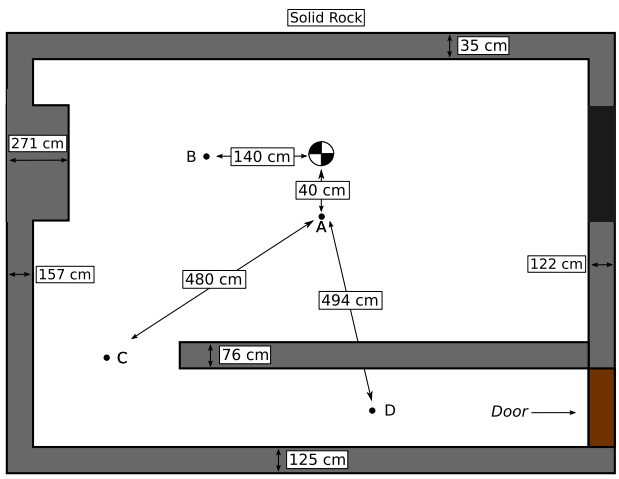

FIG. 7. Measurement locations inside the bunker of a Varian CL21EX at the Montreal General Hospital. Darker shaded regions are high density concrete, while the door is a mix of BPE and lead. Figure not to scale.

with a dose-rate of 600 MU/min and gantry positioned at 0°. The jaws were in the closed position while the multileaf collimator (MLC) remained open. Given the number of MU and the dose-rate, the spectrum at a point in air was obtained in less than 2 h including setup time.

Current-mode measurements were carried out at 40 and 140 cm from the Linac as well as at the maze-room junction and in the maze as shown in Fig. 7. All measurements were undertaken at the height of the isocenter and were completed with a total dose of 600 MU per moderator. The current produced was collected by a Keithley 6517A electrometer and converted to a count-rate using the vendor supplied calibration coefficient of 7.0 fA/(counts/s). The neutron spectrum for each location was reconstructed using our in-house MLEM unfolding software. The total fluence, ambient dose equivalent, average energy, and source strength were calculated based on the measured neutron spectra. The average energy is calculated using the lower level of the i-th energy bin.

2.E.2. Neutron dose equivalent measurements

Bubble detectors (BTI Technologies, Inc., Chalk River, Canada) were used to measure the neutron dose equivalent at the positions shown in Fig. 7 with the exception of point A. At this location, the number of bubbles produced in the detectors was so large that they become indistinguishable from one another. Two bubble detector types, PND (sensitive to neutrons with kinetic energy $E_k > 200$ keV) and BDT (sensitive to thermal neutrons) were positioned upright on a tripod at the height of the isocenter. The sum of both the PND and BDT responses provided a measure of the total neutron dose equivalent.

Neutron ambient dose equivalent was also determined from the NNS measurements. ICRP-74 fluence-to-dose coefficients[17] were used to convert the NNS-measured neutron flux spectrum into ambient dose equivalent.

2.F. Monte Carlo simulations

The Varian Clinac 21EX and bunker used for the measurements were modeled in MCNP6 (Ref. 10) using the geometry of a Varian 2300C Linac from Kase *et al.* as a template.[18] The beam shaping components and the outer shielding were updated using data from the Varian Monte Carlo Data Package (Varian Medical Systems, private communication) and physical measurements of the 21EX. The accelerator model includes the main accelerator components (target, primary collimator, flattening filter, jaws, and multileaf collimator) along with secondary components (bending magnet, waveguide, and bulk shielding).

The bunker was modeled from Montreal General Hospital blueprints with one primary barrier consisting of high density concrete (3.53 g/cm^3) while the other primary and secondary barriers were all regular concrete (2.35 g/cm^3).

The neutron fluxes at each of the points shown in Fig. 7 were calculated using the evaluated nuclear data file (ENDF) for neutron interactions and LA150U data tables for photonuclear interactions with the F5 tally in MCNP6. The starting particles were 18.0 MeV electrons with a spot size of 1.5 mm diameter incident on a tungsten target embedded in copper.

The simulation was calibrated to yield neutron fluence per Gy of photon dose at isocenter.[19] In reference conditions, 10×10 cm^2 field, 100 cm source to surface distance (SSD), and 100 cGy at the depth of maximum dose (D_{max}), the accelerator is calibrated such that 100 cGy of photon dose at D_{max} in water produces 100 MU of charge in the Linac monitor chamber. We reproduced these conditions in MCNP using a $30\times30\times30$ cm^3 water phantom with $2\times2\times1$ cm^3 voxels along the beam central axis and an upper surface at 100 cm from the source. Energy deposition by secondary electrons from photon interactions in the water was tallied (*F8 energy deposition tally) to obtain a photon percentage depth dose (PDD) curve. The MC model was tuned (by varying the electron energy) to match the simulated photon PDD with that measured using an ionization chamber. This tuning is different from the tuning of other beam models for photon therapy calculations, since the geometry is slightly different. For a tuned electron energy of 18.0 MeV, all of the measurement points were within the 2% error bars of the simulated depth dose curve. A simulation calibration coefficient was then obtained from the depth of maximum dose D_{max} of the simulated photon PDD, or 9.894×10^{-16} n/cm^2 per starting electron.

3. RESULTS

The simulated and NNS-measured spectra at different locations in the bunker are shown in Fig. 8. To reconstruct the neutron spectra, a step function (high at thermal energies and low onward) was used as input to the MLEM algorithm. This input spectrum was determined by selecting the spectrum that minimized the difference between initial and reconstructed Monte Carlo neutron spectra of a Linac. The statistical uncertainties on the measurement are shown as the shaded area around the measured spectra. However, the uncertainty (within 2%) on the simulated spectra is not shown, in order to reduce clutter.

The neutron spectrum at point A, which at 40 cm from the Linac was closest to the Linac head, shows the largest fluence-rates of all locations. A large fast neutron peak with an intermediate energy tail is present along with a smaller yet prominent thermal neutron peak. At point B, 140 cm from the isocenter, the fast neutron peak decreases while the thermal peak and intermediate energies remain relatively constant. When the measurement and simulation are moved to point C at the maze-room junction, the thermal neutron peak surpasses that of the fast neutrons. Thermal and intermediate energy neutrons are reduced by a factor of 2 while the fast neutron peak was decreased to approximately 15% of its value at 140 cm. Finally, the spectrum at point D in the maze consists mainly of thermal neutrons with a tail of intermediate energy and fast neutrons. At this location, the maximum thermal and fast neutron fluences are reduced by one and three orders of magnitude, respectively, compared to their values at point A.

Table II shows the average energy, fluence-rate, neutron source strength (Q_n), and ambient dose equivalent at points A, B, C, and D. All position dependent quantities decrease

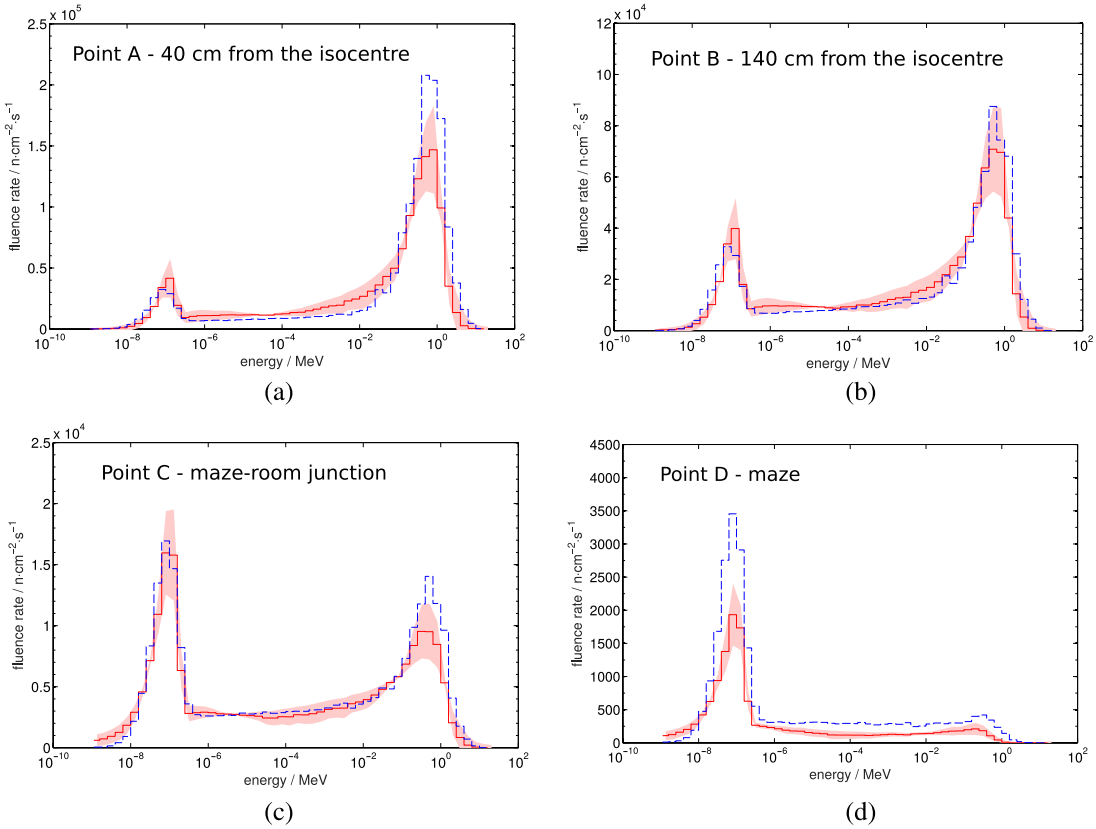

FIG. 8. Measured (solid) and simulated (dashed) neutron spectra at points A, B, C, and D in the bunker of a Varian 21EX at the Montreal General Hospital as shown in Fig. 7. The shaded region is the statistical uncertainty associated with the measurement.

as the point of measurement is displaced away from the isocenter. Q_n was calculated at point A for comparison with Howell *et al.*[16]

Fluence-rates measured using the NNS were multiplied by fluence-to-ambient dose equivalent conversion coefficients, taken from ICRP-74,[17] and integrated in energy to obtain the total ambient dose equivalent. The results are shown in Table III along with the bubble detector measurements. Dose differences as measured by the NNS and bubble detectors varied from 1% in the room to 50% in the maze.

4. DISCUSSION

In this study, the NNS, incorporating a He-3 neutron detector operated in current-mode, was found to be suitable for measuring secondary neutron spectra around a radiotherapy Linac. Current-mode operation facilitated active detector measurements in a pulsed-beam environment that would otherwise be prohibitive due to pulse pileup. Our initial performance tests, as outlined in Sec. 2.E, showed that the NNS signal was stable and that raw NNS-measured data were reproducible and linear as a function of cumulative photon dose. A neutron insensitive He-4 detector in place of the He-3 detector was used to measure photon contamination, which was determined to be negligible under the closed-jaw conditions of this study. Our custom-written MLEM unfolding algorithm was validated using vendor-supplied raw data for known neutron sources and by our own measurements using a known Am-Be source.

After unfolding with the MLEM algorithm, our NNS-measured spectra for neutrons at various locations in a treatment room, arising from a clinical 18 MV photon radiotherapy beam, were found to be consistent with expectations for both relative shape and absolute magnitude. Neutron fluence-rate

TABLE II. Average energy E_{av}, fluence-rate Φ, neutron source strength Q_n, and ambient dose equivalent $H^*(10)$ at measurement locations inside the bunker of the Varian CL21EX in 18 MV mode (600 MU/min) at the Montreal General Hospital measured using the nested neutron spectrometer. Percent uncertainties (shown in parentheses) are calculated by adding the uncertainties on each spectrum bin in quadrature.

	E_{av} (MeV)	Φ (n cm^{-2} MU^{-1})	Q_n (n Gy^{-1})	$H^*(10)$ (mSv h^{-1})
Point A	0.30	1.36×10^{5} (5.0%)	1.48×10^{12}	750.0
Point B	0.23	8.41×10^{4} (4.5%)	—	366.2
Point C	0.12	2.10×10^{4} (3.7%)	—	54.1
Point D	0.02	1.36×10^{3} (5.5%)	—	1.0

TABLE III. Neutron dose equivalent and ambient dose equivalent rates measured by bubble detectors and the NNS. ICRP-74 fluence-to-dose conversion coefficients were used to convert the NNS fluence-rates to ambient dose equivalent rates. Bubble detector measurements were not performed at point A due to the prohibitively high dose-rate.

	Point B	Point C	Point D
NNS (mSv/h)	366±40	54±5	1.0±0.2
PND+BDT (mSv/h)	390±40	62±9	2.2±0.7

decreased with distance from the source and the shape of the spectrum changed from a dominant fast neutron peak near the Linac head to a dominant thermal neutron peak in the moderating conditions of the maze. As shown in Fig. 8, relative changes in the shape of the measured spectra as a function of measurement location agreed with our Monte Carlo simulations.

In absolute terms, our NNS-measured spectra generally matched Monte Carlo predictions within the statistical uncertainty of the measurement. To calibrate our Monte Carlo neutron spectra, we generated primary photons arising from 18.0 MeV electrons under reference conditions. These primary photons were used to (a) generate photon PDD curves in a water phantom and (b) generate secondary neutron spectra at our measurement points in the treatment room and in the maze. As mentioned in Sec. 2.F, the simulated photon PDD curve matched water tank measurements for our Linac to within 2%. Absolute calibration of the Monte Carlo data was achieved by normalizing the photon dose using the known output of the Linac and scaling the secondary neutron flux accordingly. As shown in Fig. 8, there was good agreement between the absolute values of our NNS-measured neutron spectra and our Monte Carlo data. However, the simulation tended to overestimate the fast neutron component close to the head of the Linac by ~30% and the thermal neutron component in the maze by ~40%. The discrepancy in each location may be attributed to moderating hardware (shelving, furniture, and treatment accessories) present in the actual treatment room but not included in the model.

In terms of dose, neutron ambient dose equivalents calculated from our measured spectra were consistent with bubble detector measurements in the treatment room. Bubble detector measurements in the maze were compromised by the low number of neutrons there.

Our NNS-measured values for average energy, fluence-rate, neutron source strength, and ambient dose equivalent all agree to 20% with the previous work reported by Howell *et al.*[16,20] and to 40% with Kase *et al.*[18] using passive BSS measuring techniques. Table IV presents our results at 40 cm from the isocenter alongside those of Howell *et al.* and Kase *et al.* at the same location for similar Linacs. It is important to note that the values of Kase *et al.* correspond to that of a Varian 1800 lacking a MLC. Given the differences between the Linacs, we expect a lesser agreement with our results.

We note that the Linac dose-rate used in our work was 600 MU/min, where 1 MU corresponded to 1 cGy of photon dose at depth of maximum dose in water. Modern Linacs with flattening filter free beams offer a range of dose-rates that may be significantly higher than that used in this work. The effect of high dose-rate on the linearity of the NNS detector response should be investigated if employed in a flattening filter free beam.

TABLE IV. Measured average energy, fluence-rate, neutron source strength, and ambient dose equivalent from the current study and previously reported data.

	E_{av} (MeV)	Φ (n cm^{-2} MU^{-1})	Q_n (n Gy^{-1})	$H^*(10)$ (Sv MU^{-1})
Current study	0.30	1.36×10^{5}	1.48×10^{12}	2.1×10^{-5}
Howell *et al.*	0.24	1.18×10^{5}	1.26×10^{12}	1.9×10^{-5}
Kase *et al.* measured	0.42	0.8×10^{5}	—	—
Kase *et al.* calculated	0.36	1.4×10^{5}	—	—

5. CONCLUSION

Typical passive detector neutron spectrum measurements around a radiotherapy Linac require the use of thousands of MU for an adequate signal at the postirradiation readout stage. In this study, not only did we eliminate the readout stage by using an active current-mode readout but also we were able to reduce the total number of MU required for a usable signal to a fraction of the typical amount. Coupled with the practical shell design of the NNS, we were able to reliably measure the neutron spectrum at a point in less than 1 h, including setup and data unfolding. This work thus represents a new, fast, and practical method for neutron spectral measurements in radiotherapy.

ACKNOWLEDGMENTS

R. Maglieri acknowledges partial support by the CREATE Medical Physics Research Training Network grant of the Natural Sciences and Engineering Research Council (Grant No. 432290) and by the Canadian Nuclear Safety Commission (CNSC). The NNS used in this work was generously provided on loan from the CNSC. The authors wish to thank NIST and DETEC for providing the Cf-252-based NNS reference data. Helpful advice and expertise from J. Dubeau and S. Witharana at DETEC are gratefully acknowledged.

[a]Electronic mail: robert.maglieri@mail.mcgill.ca

[1]W. P. Swanson, "Radiological safety aspects of the operation of electron linear accelerators," Technical Report No. 188 (IAEA, Vienna, Austria, 1979).
[2]ICRP, "The 2007 Recommendations of the international commission on radiological protection," Technical Report No. 103 (ICRP, Ottawa, Ontario, Canada, 2007).
[3]W. D. Newhauser and M. Durante, "Assessing the risk of second malignancies after modern radiotherapy," Nat. Rev. Cancer **11**(6), 438–448 (2011).
[4]F. Brooks and H. Klein, "Neutron spectrometry—Historical review and present status," Nucl. Instrum. Methods Phys. Res., Sect. A **476**(1), 1–11 (2002).

[5]R. L. Bramblett, R. I. Ewing, and T. Bonner, "A new type of neutron spectrometer," Nucl. Instrum. Methods **9**(1), 1–12 (1960).
[6]D. S. Followill, M. S. Stovall, S. F. Kry, and G. S. Ibbott, "Neutron source strength measurements for Varian, Siemens, Elekta, and general electric linear accelerators," J. Appl. Clin. Med. Phys. **4**, 189–194 (2003).
[7]R. Barquero, R. Méndez, M. Iniguez, H. Vega-Carrillo, and M. Voltchev, "Thermoluminescence measurements of neutron dose around a medical linac," Radiat. Prot. Dosim. **101**(1-4), 493–496 (2002).
[8]J. Dubeau, S. S. Hakmana Witharana, J. Atanackovic, A. Yonkeu, and J. P. Archambault, "A neutron spectrometer using nested moderators," Radiat. Prot. Dosim. **150**, 217–222 (2012).
[9]M. Hagiwara *et al.*, "Shielding experiments at high energy accelerators of Fermilab (III): Neutron spectrum measurements in intense pulsed neutron fields of the 120-GeV proton facility using a current Bonner sphere technique," Prog. Nucl. Sci. Technol. **1**, 52–56 (2011).
[10]Los Alamos National Laboratory, MCNP6 Users Manual–Code Version 6.1.1beta, June 2014.
[11]L. A. Shepp and Y. Vardi, "Maximum likelihood reconstruction for emission tomography," IEEE Trans. Med. Imaging **1**(2), 113–122 (1982).
[12]F. Perey, Least-squares dosimetry unfolding: The program STAY'SL, ORNL/TM-6062, 1977.
[13]H. R. Vega-Carrillo, E. Manzanares-Acuña, M. P. Iñiguez, E. Gallego, and A. Lorente, "Study of room-return neutrons," Radiat. Meas. **42**(3), 413–419 (2007).
[14]H. R. Vega-Carrillo, E. Manzanares-Acuña, M. P. Iñiguez, E. Gallego, and A. Lorente, "Spectrum of isotopic neutron sources inside concrete wall spherical cavities," Radiat. Meas. **42**(8), 1373–1379 (2007).
[15]International Standards Organization, "Reference neutron radiations-Part 1: Characteristics and methods of production," Technical Report No. ISO-8529-1 (International Organization for Standardization, Geneva, Switzerland, 2001).
[16]R. M. Howell, S. F. Kry, E. Burgett, N. E. Hertel, and D. S. Followill, "Secondary neutron spectra from modern Varian, Siemens, and Elekta linacs with multileaf collimators," Med. Phys. **36**, 4027–4038 (2009).
[17]International Commission on Radiological Protection, "Conversion coefficients for use in radiological protection against external radiation," Technical Report No. 74 (ICRP Publication, International Organization for Standardization, Ottawa, Ontario, Canada, 1996).
[18]K. Kase, X. Mao, W. Nelson, and J. Liu, "Neutron fluence and energy spectra around the Varian Clinac 2100C/2300C medical accelerator," Health Phys. **74**, 38–47 (1998).
[19]H. R. Vega-Carrillo, S. A. Martínez-Ovalle, A. M. Lallena, G. A. Mercado, and J. L. Benites-Rengifo, "Neutron and photon spectra in Linacs," Appl. Radiat. Isot. **71**, 75–80 (2012).
[20]R. M. Howell, S. F. Kry, E. Burgett, N. E. Hertel, and D. Followill, "Erratum: 'Secondary neutron spectra from modern Varian, Siemens, and Elekta linacs with multileaf collimators' [Med. Phys. 36(9), 4027–4038 (2009)]," Med. Phys. **38**(12), 6789 (2011).